# TIME-DISTANCE HELIOSEISMOLOGY WITH THE MDI INSTRUMENT: INITIAL RESULTS


T. L. DUVALL JR.
*Laboratory for Astronomy and Solar Physics,*
*NASA Goddard Space Flight Center, Greenbelt, MD 20771, USA*

A.G. KOSOVICHEV, P.H. SCHERRER, R.S. BOGART, R.I. BUSH,
C. DE FOREST, J.T. HOEKSEMA and J. SCHOU
*W.W. Hansen Experimental Physics Laboratory,*
*Stanford University, Stanford, CA 94305, USA*

J.L.R. SABA, T.D. TARBELL, A.M. TITLE and C.J. WOLFSON
*Lockheed-Martin Advanced Technology Center*
*91-30/252, 3251 Hanover St., Palo Alto, CA 94304.*

and

P.N. MILFORD
*Parallel Rules*
*41 Manzanita Ave., Los Gatos, CA 95030*



**Abstract.** In time-distance helioseismology, the travel time of acoustic waves is measured between various points on the solar surface. To some approximation, the waves can be considered to follow ray paths that depend only on a mean solar model, with the curvature of the ray paths being caused by the increasing sound speed with depth below the surface. The travel time is affected by various inhomogeneities along the ray path, including flows, temperature inhomogeneities, and magnetic fields. By measuring a large number of times between different locations and using an inversion method, it is possible to construct 3-dimensional maps of the subsurface inhomogeneities.

The SOI/MDI experiment on SOHO has some unique capabilities for time-distance helioseismology. The great stability of the images observed without benefit of an intervening atmosphere is quite striking. It has made it possible for us to detect the travel time for separations of points as small as 2.4 Mm in the high-resolution mode of MDI (0.6 arcsec/pixel). This has enabled us to detect the supergranulation flow. Coupled with the inversion technique, we can now study the 3-dimensional evolution of the flows near the solar surface.


## 1. Introduction

Three strong features of the MDI instrument on SOHO (Scherrer *et al.* 1995) are the stability coming from the absence of an intervening atmosphere between the telescope and the Sun, an orbit in continuous sunlight enabling long sequences of 'around-the-clock' observing, and the relatively high resolution compared to some groundbased helioseismology experiments. In this paper, we describe work that fully exploits these features of MDI and which points to a future in which we will be able to follow in detail the subsurface convection.

We are using a new technique coming to be known as time-distance helioseismology (Duvall *et al.* 1993; Duvall *et al.* 1996*a*, *b*; Kosovichev 1996; Kosovichev and Duvall, 1996; D'Silva 1996; D'Silva *et al.* 1996), in which the time $t(x1, x2)$ for acoustic waves to travel between different surface locations $(x1, x2)$ is measured from a cross correlation technique. In the first approximation, the time $t(x1, x2)$ depends on inhomogeneities along a geometric ray path connecting the surface locations. If the temperature is locally high, the waves will traverse the region more quickly leading to a shorter time. If there is a flow with a component in the direction of the ray path, the flow will tend to speed up the wave in the direction of the flow, while slowing it down in the reciprocal direction. In this case, we are lead to the very distinctive signature of the travel time being different for the opposite direction of travel between the same points. We have found no other effect which can yield this signature.

A magnetic field in the region of wave travel can also lead to travel time anisotropy (Duvall *et al.* 1996*a*). These are somewhat harder to isolate, as the distinctive signature of the field is that waves travelling along the field direction have a different wave speed than waves travelling perpendicular to the field. For some field geometries, it is possible to set up pairs of rays that intersect at right angles to look for this type of signature, but it is more difficult as the two rays have different paths except at the location where they intersect, and so other inhomogeneities can confuse the issue. The general form of rays below the surface is shown in Fig. 4. In this paper the effect of magnetic anisotropy is not considered.

## 2. Observations

For this study we have used 8.5 hours of Doppler images from January 27, 1996 taken in the high resolution mode of MDI, which has 0.6 arcsec/pixel. To study convection near the surface, it is necessary to use fairly short intervals in order that the evolution not be too great during the observing interval. On the other hand, it is necessary to observe for some length of time in order to get a statistical sample of waves. The 8.5 hours is a compromise between these two competing requirements, with the supergranule lifetime of about 1 day putting an upper limit on how long to observe. Another point is that we need to observe for longer than the travel time as the correlation that we are detecting arises from the same wave travelling from one location to the other through the subsurface layers. The travel times used in the present study are for surface point separations in the range 6-30 Mm, and are in the interval 17-34 minutes.

An example of a Doppler image is shown in Fig. 1. There is considerable high spatial frequency information in the image, as measurements of the point-spread function of the instrument would predict (Scherrer *et al.* 1995).

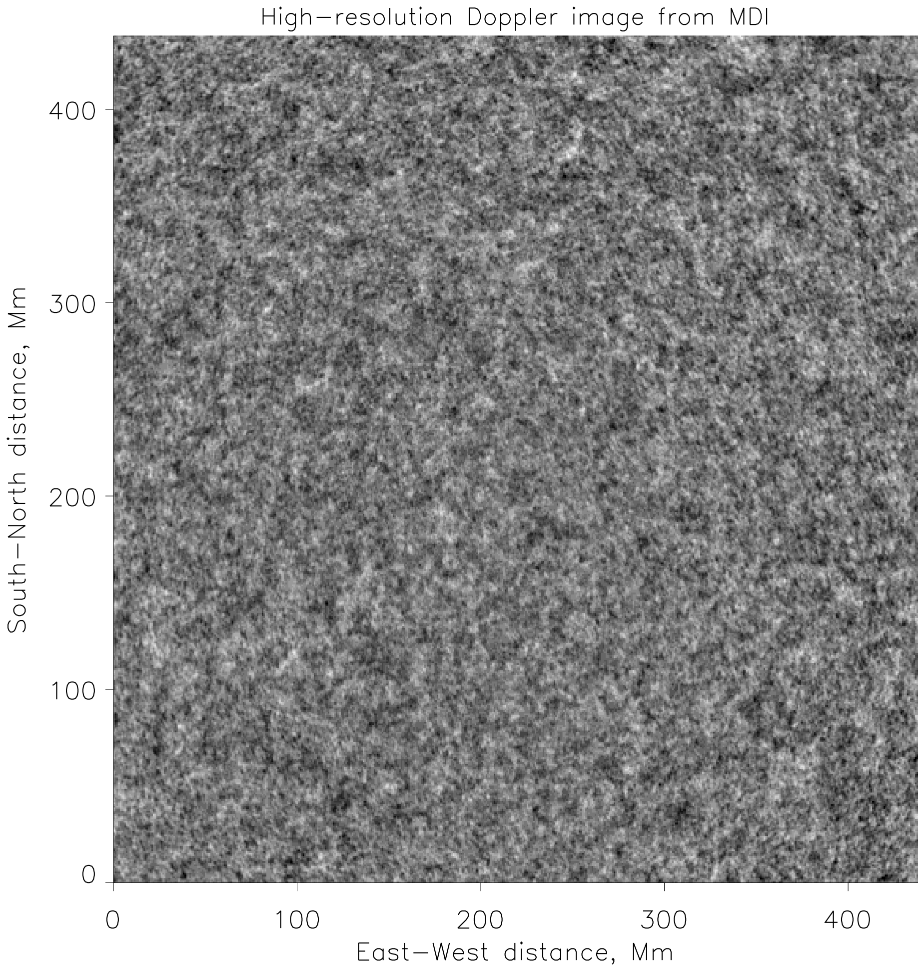


Fig. 1. A MDI Dopplergram for the high resolution field on 27 Jan. 1996. White is for receding velocity, black for approaching. The solar rotation has been removed. The image is dominated by the p-mode oscillations and granulation. The standard deviation of the velocity values is 244 m/s.

And in fact, with 0.6 arcsec/pixel we are somewhat oversampling the p-mode signal. With this sampling the spatial nyquist frequency is near spherical harmonic degree $l = 5000$. But the fundamental mode, the lowest frequency mode in the p-mode range, crosses the peak acoustic cutoff frequency ($\sim 5.3$ mHz) at degree $l = 2700$. Since the peak of the power envelope is near temporal frequency 3.2 mHz, there is very little power due to oscillations in the outer half (in spatial frequency) of the power spectrum. We have used this information explicitly in some later experiments in which the images are binned 2x2 on board the SOHO spacecraft to reduce the telemetry required.

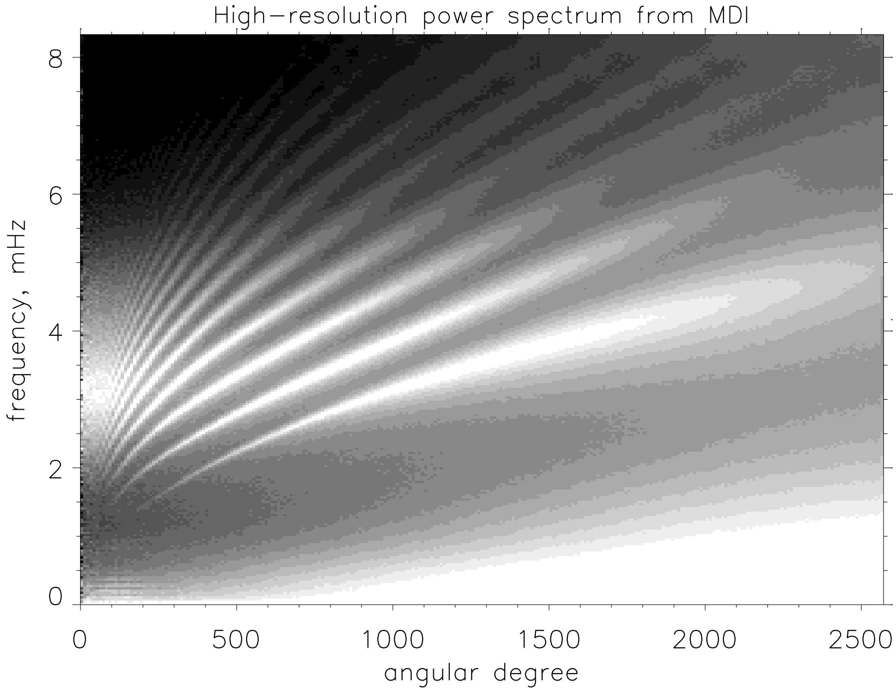


Fig. 2. A mean power spectrum for the 8.5 hour interval studied on 27 Jan. 1996. The solar rotation was removed before the power spectrum was computed. The raw data was binned 2x2 before the analysis, so the spatial nyquist frequency shown is half of the possible, although we get almost all the oscillation signal with the present analysis. The power spectrum is smooth because it has been averaged over wave direction.

The mean power spectrum of the 8.5 hours of data is shown in Fig. 2. The spectrum is smooth as it has been averaged over azimuth. The spatial frequency response has been flattened to remove the effects of the point-spread function. The excellent quality of the data is apparent. One striking thing is the large width of the f mode, which increases to $\sim$1 mHz (full-width at half maximum) in width at $l = 2500$. It seems likely that much of this width could be caused by motions at the surface causing the waves to be Doppler shifted. Using the standard Doppler-shift relation, $v = \Delta\omega/k$, we find a flow velocity, $v$, of 0.9 km/s for a frequency shift, $\Delta\omega/2\pi$, of 0.5 mHz (one half of full-width at half maximum), and for a horizontal wave number, $k = \sqrt{l(l+1)}/R_{\odot}$. This is of the order of surface motions from convection, as seen by correlation tracking or as seen later in this paper by the time-distance technique.

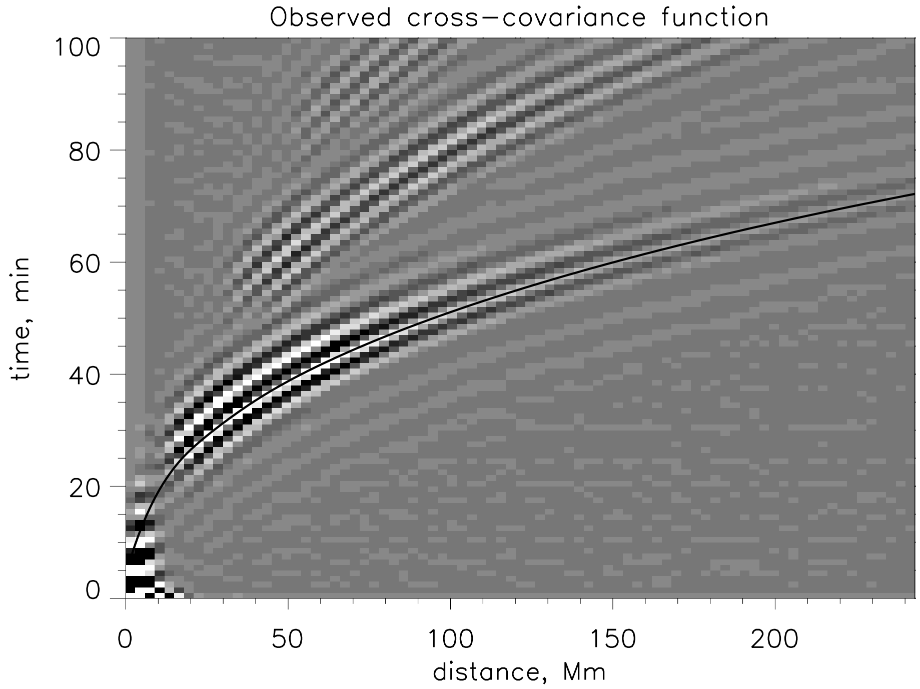


Fig. 3. A mean cross covariance function for the data. The solid line is a theoretical plot of the time for waves to travel along a ray path for the specified great-circle distance. The grayscale picture is the cross covariance function. The first, second and third bounces are visible near 30 min., 60 min., and 90 min. The fine structure in each of the ridges is caused by the finite bandpass of the oscillations.

## 3. Analysis

To get the travel times between different locations, we calculate the temporal cross correlation function between the data at one location and the data within an annulus at some great-circle distance from the point. We look at both positive and negative lags of the correlation function, as this can tell us in which direction the waves are travelling. For example, a signal at location 1 first and at location 2 later will lead to a signal at one sign of lag while a signal at location 2 first will lead to a correlation at the opposite sign of lag.

The cross correlation function, averaged over a number of origins, is shown in Fig. 3, along with a curve showing the time versus distance for a simple theory. If we imagine generating a pulse of acoustic energy at the surface that propagates along the ray paths to the distant location, we might expect to see a pulse at the distant location. But in fact we see something that is much broader and really looks like a wave packet with a period of five minutes, and a width in time of about 1/bandwidth of our oscillation power spectrum, or $(1\ \mathrm{mHz})^{-1}$=17 min. This makes sense, because the pulse that we generated at the surface had an infinite bandwidth and so could make a zero-width feature in the correlation function. As shown earlier by Duvall *et al.* (1993), the correlation function that we observe is the Fourier transform of the power spectrum (e.g. Fig. 2). The remaining features in Fig. 3 correspond to the multiple bounces. If there is a correlation observed at time $t$ and at distance $d$, there will be a similar signal at $n \times t$ and $n \times d$, where $n$ is integral.

In some earlier work (Duvall *et al.* 1993), the correlation function was rectified by using the analytic signal formalism, and times were measured from this signal which is the envelope of the correlation function. Later it was found that the higher frequency structure in the correlation function actually is a more sensitive measure of subsurface inhomogeneities (Duvall *et al.* 1996*a*). In that work, the location of one of the fine structure peaks was determined by measuring the zero crossing of the instantaneous phase of the correlation function. For the present work, this has been further refined (Kosovichev and Duvall 1996). A 20-minute interval in the neighborhood of the peak in the correlation function is fit to a Gaussian wave packet, with independent parameters for the location of the envelope, the location of one of the fine structure peaks, the amplitude and width of the Gaussian, and the frequency. All the results shown are from the location of the fine structure peak.

In Fig. 4, we show some examples of raypaths below the surface. The ray paths are curved because of the increasing sound speed with depth in the Sun. A rule of thumb that we have found useful is that the horizontal distance of the ray between surface reflections is given approximately by $\pi$ multiplied by the depth of the turning point of the ray. This relation is exactly true for a polytrope and approximately true for a real solar model. Also the length of the ray is four times the depth.

Following Duvall *et al.*(1996*a*), we compute the mean cross correlation for waves travelling both out from the center to the annuli and the reverse. The difference of the times measured from these cross correlations is a measure of divergence of the flow. It could be due to either a downflow near the central location or to an average horizontal outflow (or inflow) near the annulus. In addition to this divergence signal, a mean time is computed for the inward and outward waves. To get more directional information about flows, we break up the annulus surrounding a point into quadrants, centered on the four directions north, south, east, west (Duvall *et al.* 1996*b*). We then average the cross correlations for eastward and westward waves separately. The travel times are measured separately for the eastward and westward waves by the above procedure. To get a signal proportional to a flow, we then take the difference of these two times. The same procedure is applied to north-south propagation.

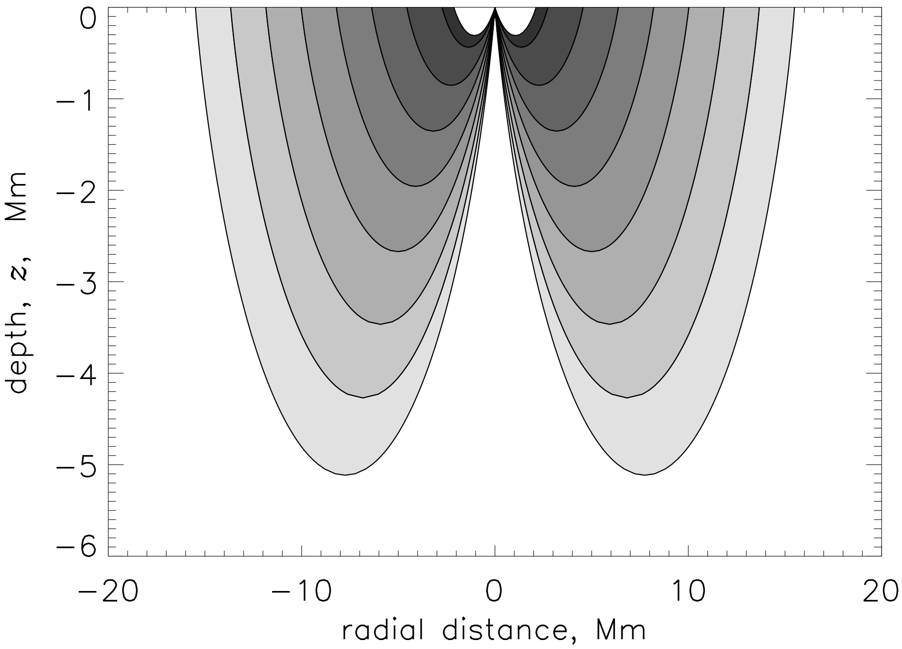


Fig. 4. The rays going from the center to the different annuli. The ray paths are curved because of the increasing sound speed with depth. The sound speed increases from 7 km/s near the surface to 35 km/s at 10 Mm depth. The horizontal separation between surface points is approximately $\pi$ times the depth. The measured travel times are sensitive to the component of velocity along the particular ray path.

In Fig. 5 we show the four different sets of times computed for each range of distance: i) outward-inward, ii) west-east, iii) north-south, and iv) mean time. These 32 images are the input to the inversion described next. In general, the signals for the smaller annuli should be more sensitive to near-surface inhomogeneities. The cellular pattern with the scale size of supergranulation is most apparent in the outward-inward signal. Of course, the rays focus at the center points at the surface, but also reach the surface in the annuli. One interesting thing to notice is the apparent large scale patterns visible in the signals from the larger annuli. What we cannot distinguish directly is whether these patterns are due to large scale signals near the surface which are being picked by the annular filter or are due to larger scale flows near the bottom of the ray paths being seen because the rays for the larger annuli are penetrating deeper. In principle the inversion is able to distinguish between these choices, but it would be useful to have another way to see this. Maybe in future work the signal from the second bounce could be used to make this distinction.

To check that we are seeing something with a basis in reality, we have

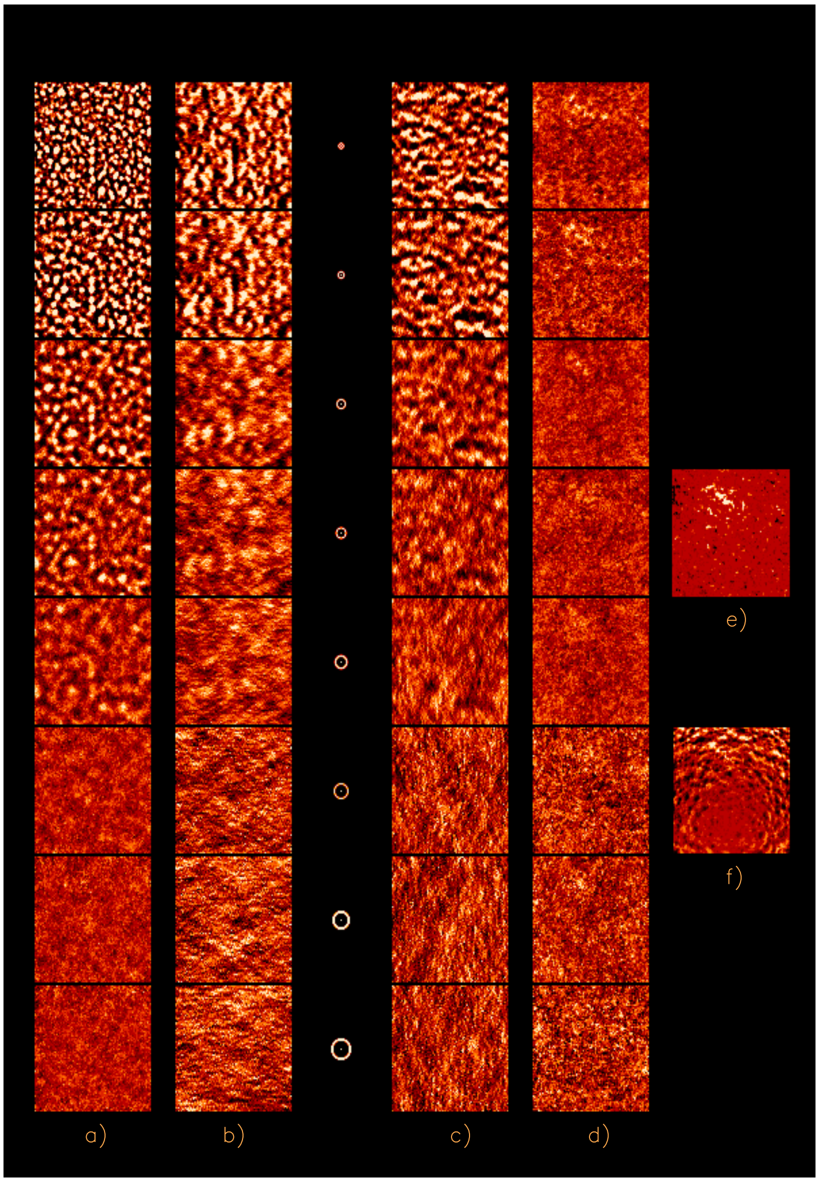


Fig. 5. Maps of the times measured and input to the inversion procedure. The 8 pictures vertically are for the 8 different annulus sizes. The sizes of the annuli are shown in the central column, smallest at the top and largest at the bottom. The horizontal size of each image is 370 Mm. a) Time for outward-going waves minus inward-going waves with white displayed as a negative signal. The rms signal in the top image is 0.2min while in the bottom one is 0.04min. b) Westward times minus eastward times. The rms signal in the top image is 0.35min. while in the bottom image is 0.19min. c) Northward times minus southward times. The magnitudes are similar to b). d) The variation in mean time for the average of inward and outward times with a negative signal displayed as white. The rms of the top image is 0.05min. while for the bottom image it is 0.08min. A correlation of this signal with the location of the magnetic features can be seen, in agreement with that seen by Duvall *et al.* (1996$a$, $b$). e) The magnetic field in this region, as observed with the MDI instrument. f) The mean Doppler signal observed for the 8.5 hour interval. This shows mainly the horizontal motions of supergranules. Near the center of the disk (lower center of picture) the signal from horizontal flows disappears because it is perpendicular to the line of sight.

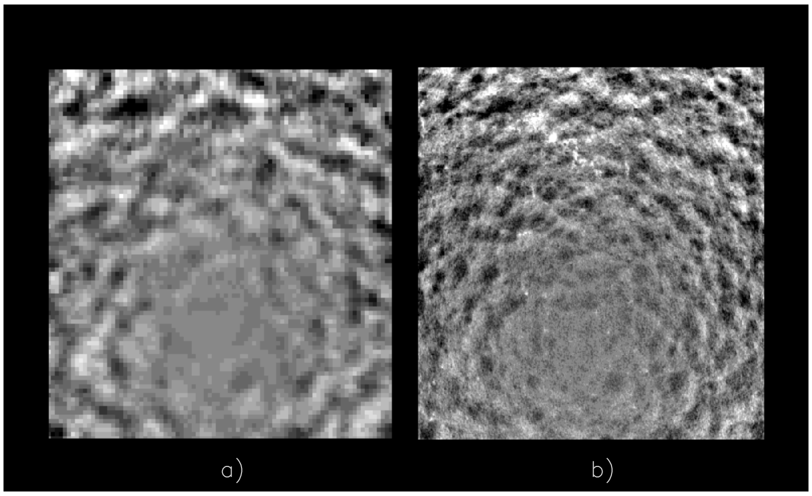


Fig. 6. A comparison between a simulated Doppler image using the images from the top line of Fig. 5 ( b) and c) ) and the mean Doppler image for the 8.5 hours (Fig. 5 f) ). a) The simulated image. The east-west and north-south times are combined and then projected onto the line of sight. b) The mean Doppler image for the 8.5 hours.

used the west-east and north-south signals for the smallest annulus to make an apparent horizontal velocity to compare with the mean Doppler image over the 8.5-hour period. The west-east and north-south times are taken as the components of a horizontal vector and the line-of-sight component of this vector is taken. The times are calibrated using the mean sound speed over the depth range of the rays from a solar model. The comparison between these two is shown in Fig. 6. The very high correlation is apparent. The correlation coefficient between these two images is 0.74. The signals disappear near the disk center because the supergranulation velocity is predominantly horizontal which is perpendicular to our line of sight at disk center.

Another check on our understanding is shown Fig. 7. The same components of east-west and north-south velocity used in Fig. 6 are combined to show horizontal velocity vectors. The vectors are overlaid on an image of the absolute value of magnetic field. We see that the magnetic field tends to lie at the boundaries of the cellular outflows, in agreement with our general picture of the magnetic network.

The images are used in a ray-theory inversion (Kosovichev 1996, Kosovichev and Duvall 1996). The region of the Sun is separated into a 3-D grid of inhomogeneities with the same horizontal sampling interval as the input images (4.3Mm) and an equal increment in depth covering the same depth

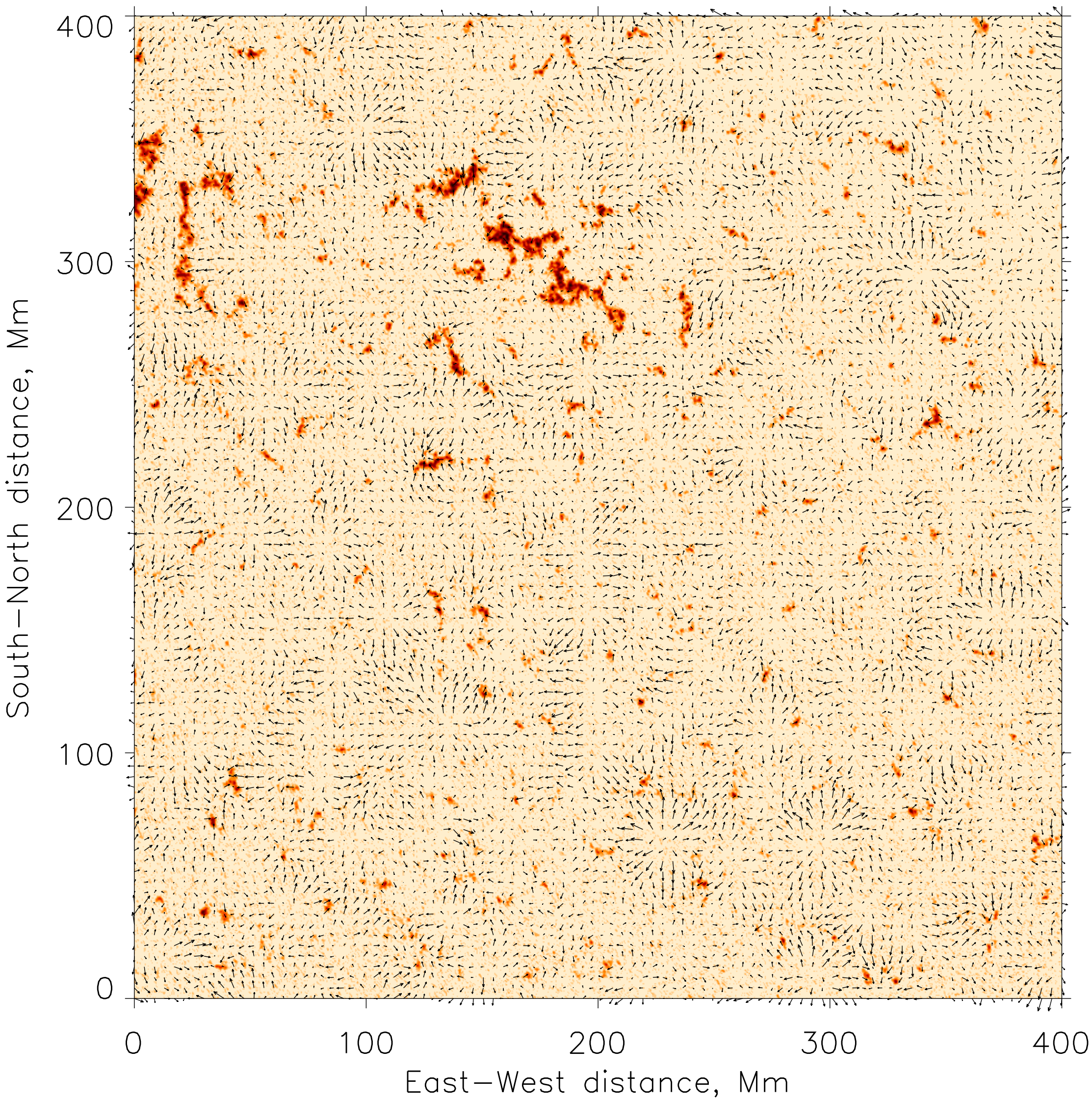


Fig. 7. A comparison between the absolute value of magnetic field (in color) and the simulated velocity from the time-distance pictures (arrows). The longest arrow is for 1 km/s velocity.

range as the input data. The number of grid points in depth is taken to be the same as the number of input images, and, in this case, is 8. Each grid point has four independent variables, the three components of flow velocity and a sound speed inhomogeneity. No attempt is made to satisfy any conservation equations, like the continuity equation.

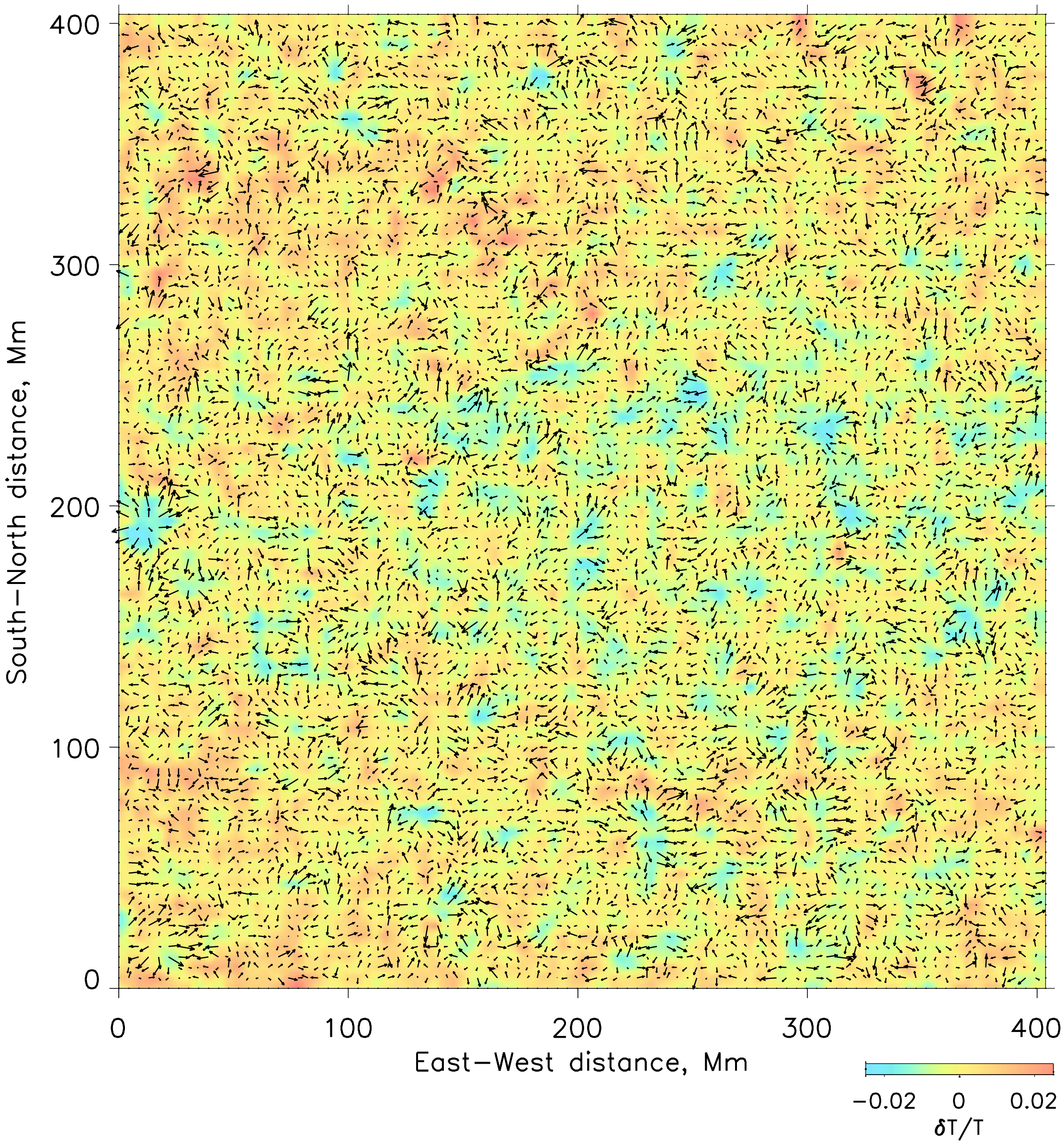


Fig. 8. The horizontal flows near the surface from the inversion procedure are shown as vectors. The vectors are overlaid on the inverted temperature structure shown in blue and red for hotter and cooler.

In Fig. 8, we show the inversion results for the surface layer. The high correlation with the mean Doppler image is apparent. One advantage of studying near-surface regions is that we do have extra information at the surface that we would not have for the deep interior. So we have a check on

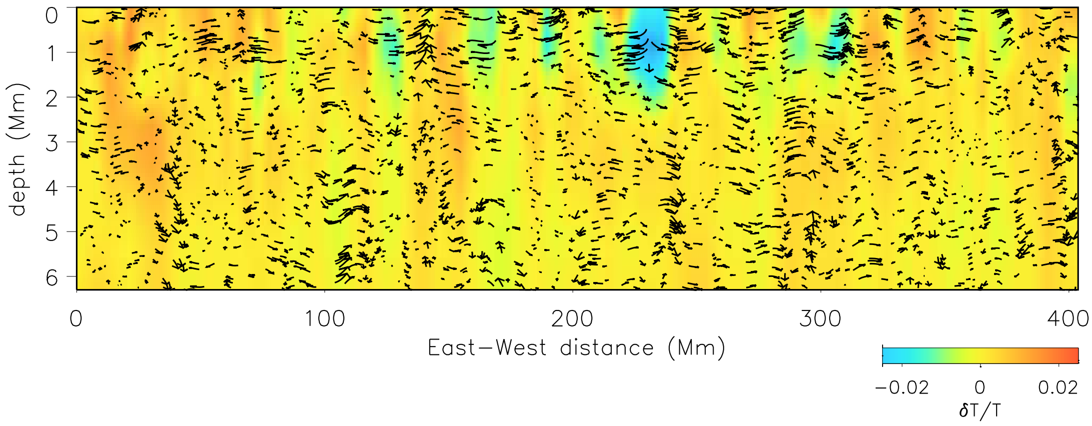


Fig. 9. A vertical cut showing the component of flow in the plane. The flow is again shown as vectors and is overlaid on the temperature inhomogeneities.

the results.

In Fig. 9 we show a vertical cut showing the subsurface flows and sound speed inhomogeneities. It would appear that the pattern of horizontal motions at the surface only persists to a few Megameters in depth. But it is probably premature to draw strong conclusions yet because of the newness of the method.

## Conclusions

We have shown that there is detailed information about the subsurface inhomogeneities contained in the helioseismology data. We have also shown it should be possible to extract this information and have shown some 1st order attempts to do so. We would appear to have an exciting new window into the solar interior.

## Acknowledgments

This research is supported by the SOI-MDI NASA contract NAG5-3077 at Stanford University.

## References

D'Silva, S., 1996, *Astrophys. J.*, 469, 964.
D'Silva, S., Duvall, T.L.Jr., Jefferies, S.M. & Harvey, J.W., *Astrophys. J.*, 471, 1030.
Duvall, T.L.Jr., Jefferies, S.M., Harvey, J.W., & Pomerantz, M.A., 1993, *Nature*, 362, 430.
Duvall, T.L.Jr., D'Silva, S., Jefferies, S.M., Harvey, J.W., & Schou, J., 1996*a*, *Nature*, 379, 235.

Duvall, T.L.Jr., Kosovichev, A.G., Scherrer, P.H., & Milford, P.N., 1996*b*, *BAAS*, 188, 49.08

Kosovichev, A.G., 1996, *Astrophys. J.*, 461, L55.

Kosovichev, A.G. & Duvall, T.L.Jr., 1996, in: "Solar Convection and Oscillations and their Relationship", eds J. Christensen-Dalsgaard and F. Pijpers, Proc. of SCORe'96 Workshop, Aarhus (Denmark), May 27-31, 1996, Kluwer Acad. Publ, in press.

Scherrer, P.H., Bogart, R.S., Bush, R.I., Hoeksema, J.T., Kosovichev, A.G., Schou, J., Rosenberg, W., Springer, L., Tarbell, T.D., Title, A., Wolfson, C.J., Zayer, I., and the MDI Engineering Team, 1995, *Solar Phys.*, 162, 129.